

**SYNTHESIS, CHARACTERIZATION AND  
CATALYTIC STUDY OF MICROPOROUS  
SILICOALUMINOPHOSPHATES IN THE  
ESTERIFICATION OF LEVULINIC ACID  
WITH ETHANOL**

**MA YIK KEN**

**UNIVERSITI SAINS MALAYSIA**

**2022**

**SYNTHESIS, CHARACTERIZATION AND  
CATALYTIC STUDY OF MICROPOROUS  
SILICOALUMINOPHOSPHATES IN THE  
ESTERIFICATION OF LEVULINIC ACID WITH  
ETHANOL**

by

**MA YIK KEN**

**Thesis submitted in fulfilment of the requirements  
for the degree of  
Master of Science**

**July 2022**

## ACKNOWLEDGEMENT

First and foremost, I would like to express my deepest appreciation towards my supervisor, Associate Professor Dr. Ng Eng Poh for his tireless patience, deep knowledge and expertise throughout my entire project. Without his continuous guidance and supervision, I would not have completed my Master's studies with such ease. Besides, I would also like to thank immensely my seniors, Dr Hidayahni and Dr Ismail Alhassan, in assisting and providing useful advice on my studies. I have greatly benefitted from their help and deepened my knowledge on zeolites.

I would also like to extend my gratitude to the School of Chemical Sciences, Universiti Sains Malaysia (USM), and Global Archaeological Research Centre for providing and allowing the usage of their facilities for analysis during my course of study here. Special thanks to all academic, technical and administrative staff in assisting and facilitating my studies especially during this trying time. I would also like to thank Research University grant (RUI1001/PKIMIA/8011128) and GRA-Assist (2020) for the financial support given that has greatly alleviated my burden.

Last but not least, my sincerest gratitude is dedicated to my parents whose unconditional support, love and motivation have been the pillar of my strength without which I could not possibly have completed my Master's research. Special mention of my friends, Mr. Choong Zheng Yi for his assistance throughout my studies in USM.

## TABLE OF CONTENTS

<b>ACKNOWLEDGEMENT .....</b>	<b>ii</b>
<b>TABLE OF CONTENTS.....</b>	<b>iii</b>
<b>LIST OF TABLES .....</b>	<b>vii</b>
<b>LIST OF FIGURES .....</b>	<b>viii</b>
<b>LIST OF SYMBOLS, ABBREVIATION AND NOMENCLATURES....</b>	<b>xii</b>
<b>ABSTRAK.....</b>	<b>xiv</b>
<b>ABSTRACT .....</b>	<b>xvi</b>
<b>CHAPTER 1 INTRODUCTION.....</b>	<b>1</b>
1.1 General introduction .....	1
1.2 Research objectives .....	4
1.3 Thesis outline.....	5
<b>CHAPTER 2 LITERATURE REVIEW.....</b>	<b>7</b>
2.1 Zeolites as microporous materials .....	7
2.2 Zeolites and silicoaluminophosphate (SAPO-n) zeotype materials ....	8
2.2.1 Zeolites.....	8
2.2.2 Aluminophosphate (AlPO-n) and silicoaluminophosphate (SAPO-n) zeotypes .....	12
2.2.3 Mechanism of Si insertion .....	14
2.2.4 Structural building units, topology codes and framework structures .....	16
2.2.5 Comparison between zeolites and SAPO-n zeotype materials .....	18
2.3 Hydrothermal synthesis .....	20
2.3.1 Effect of synthesis parameters .....	21

2.3.2	Roles of organic SDAs.....	23
2.3.3	Mechanism of crystallization.....	26
2.3.3(a)	Solution-mediated transport mechanism.....	26
2.3.3(b)	Solid hydrogel transformation mechanism.....	27
2.3.3(c)	Autocatalytic nucleation mechanism.....	28
2.4	Silicoaluminophosphate number 34 (SAPO-34) zeotype.....	29
2.4.1	Factors affecting the formation of SAPO-34 zeotype.....	30
2.4.1(a)	Effect of the nature and the concentration of organic SDAs.....	30
2.4.1(b)	Effects of the crystallization temperature and time.....	33
2.4.1(c)	Effects of the concentration and sources of silica	34
2.4.1(d)	Effects of the phosphorus and water content.....	35
2.5	Silicoaluminophosphate number 35 (SAPO-35) zeotype.....	36
2.6	Removal of organic structural directing agents (SDAs).....	38
2.7	Catalytic esterification of levulinic acid.....	39
2.7.1	Levulinic acid (LA).....	39
2.7.2	Ethyl levulinate (EL) ester.....	41
2.7.3	Synthesis of ethyl levulinate (EL).....	42
2.7.4	Heating methods.....	45
2.7.4(a)	Reflux method.....	45
2.7.4(b)	Autoclave heating method.....	45
2.7.4(c)	Microwave heating method.....	46
2.7.4(d)	Non-microwave instant heating method.....	47
2.8	Summary.....	50

<b>CHAPTER 3</b>	<b>MATERIALS AND EXPERIMENTAL METHODS....</b>	<b>51</b>
3.1	Preparation of 1-propylpyridinium hydroxide ([PPy]OH) template solution.....	51
3.2	Crystallization of SAPO-34 .....	52
3.3	Crystallization of SAPO-35 .....	53
3.4	Characterization techniques .....	54
3.4.1	X-ray powder diffraction (XRD) .....	54
3.4.2	Field emission scanning electron microscopy (FESEM) ....	54
3.4.3	Fourier transform infrared spectroscopy (FTIR) .....	55
3.4.4	Nitrogen (N <sub>2</sub> ) gas adsorption-desorption analysis .....	56
3.4.5	Inductively coupled plasma optical emission spectroscopy (ICP-OES) .....	58
3.4.6	Temperature programmed desorption of ammonia (NH <sub>3</sub> -TPD) analysis .....	59
3.4.7	Thermogravimetric-differential thermogravimetric analysis (TG/DTG) .....	60
3.4.8	CHNS/O elemental analysis.....	60
3.4.9	Nuclear magnetic resonance (NMR) spectroscopy .....	61
3.4.10	Gas chromatography (GC) .....	62
3.4.11	Gas chromatography-mass spectrometry (GC-MS).....	64
3.5	Catalytic esterification of levulinic acid with ethanol .....	64
<b>CHAPTER 4</b>	<b>RESULTS AND DISCUSSION .....</b>	<b>67</b>
4.1	Overview.....	67
4.2	Characterization of 1-propylpyridinium bromide, [PPy]Br .....	68
4.3	Time-dependent formation of SAPO-34 .....	71

4.4	Time-dependent formation of SAPO-35 .....	85
4.5	Catalytic esterification of levulinic acid with ethanol .....	95
4.5.1	Effect of catalyst loading .....	96
4.5.2	Effect of the molar ratio of levulinic acid with ethanol .....	97
4.5.3	Effects of temperature and time .....	98
4.5.4	Effects of alcohol chain length and branching .....	101
4.5.5	Effect of heating mode .....	102
4.5.6	Catalysts comparative study .....	103
4.5.7	Proposed mechanism .....	105
4.5.8	Catalysts reusability study .....	107
<b>CHAPTER 5 CONCLUSION AND RECOMMENDATIONS .....</b>		<b>109</b>
5.1	Conclusions .....	109
5.2	Recommendations .....	110
<b>REFERENCES .....</b>		<b>112</b>

## **APPENDICES**

### **LIST OF PUBLICATIONS**

## LIST OF TABLES

		<b>Page</b>
Table 2.1	The industrial applications of zeolites .....	11
Table 2.2	The structure types, pore sizes and pore openings of several AlPO-n.....	13
Table 2.3	Some SAPO-n materials with their respective structure codes, ring openings and framework structure.....	17
Table 2.4	A comparison between the zeolites and the SAPO-n zeotypes	19
Table 2.5	A comparison of the synthesis condition of SAPO-34 .....	32
Table 2.6	The physical properties of levulinic acid at 293 K.....	39
Table 2.7	Some of the important physical properties of ethyl levulinate as a biofuel additive .....	42
Table 2.8	Esterification reaction of LA with ethanol into EL in the presence of various catalysts using conventional reflux heating method .....	44
Table 2.9	A comparison of conversion efficiency in various organic reactions using microwave and non-microwave instant heating method .....	48
Table 3.1	The possible vibration bands of zeolites in the IR fingerprint region .....	56
Table 3.2	GC oven and measurement conditions.....	63
Table 4.1	Elemental composition of [PPy]Br.....	69
Table 4.2	Crystalline phase, chemical composition, porous and acid properties of solid samples treated at various times.....	82
Table 4.3	Chemical composition and acidity of SAPO-35 .....	94
Table 4.4	The effect of heating mode on the esterification of LA. Reaction conditions: Temperature = 190 °C, time = 20 min, LA = 1.33 mmol, EtOH = 14.7 mmol, mass of SAPO-34 catalyst = 0.100 g. Number of experiment = 2.....	103



## LIST OF FIGURES

		<b>Page</b>
Figure 2.1	The random combination of primary building units (PBUs) into the secondary building units (SBUs) and the connection among the SBUs into zeolites of different framework types (R = ring, D4R = double 4 ring, D6R = double 6 ring) .....	10
Figure 2.2	A general two-dimensional structure of a zeolite framework .	10
Figure 2.3	A neutral framework of aluminophosphate (AlPO-n) with alternating $[AlO_4]^-$ and $[PO_4]^+$ monomer units .....	12
Figure 2.4	Three substitution mechanisms of silicon into a AlPO-n framework .....	16
Figure 2.5	Schematic diagram of the preparation procedure and the hydrothermal synthesis of SAPO-n zeotypes.....	21
Figure 2.6	Schematic illustration of the solution-mediated transport of the zeolite crystallization mechanism.....	26
Figure 2.7	Schematic illustration of the solid-phase transformation mechanism .....	27
Figure 2.8	Schematic illustration of the autocatalytic nucleation mechanism .....	28
Figure 2.9	(a) The diameter of the eight-membered ring and (b) the framework structure of SAPO-34 viewed normal to [001] ....	29
Figure 2.10	Several organic SDAs used for the crystallization of SAPO-34.....	31
Figure 2.11	(a) The diameters of the eight-membered pores and (b) the framework of SAPO-35 viewed normal to [001] .....	36
Figure 2.12	Some organic SDAs used to crystallize SAPO-35.....	37
Figure 2.13	The derivatives of levulinic acids and their respective industrial applications .....	40
Figure 2.14	The synthesis of ethyl levulinate <i>via</i> esterification of levulinic acid with ethanol in the presence of an acid catalyst .....	43
Figure 2.15	Schematic illustration of a Teflon-lined stainless-steel autoclave .....	46

Figure 2.16	(a) Anton Paar's Monowave 50 reactor and (b) schematic diagram of this non-microwave instant heating reactor .....	47
Figure 3.1	Schematic illustration to produce 1-propylpyridinium hydroxide.....	52
Figure 3.2	Types of adsorption isotherm curves classified by IUPAC ....	58
Figure 3.3	Flowchart of the experimental procedure in this project .....	66
Figure 4.1	FT-IR spectrum of [PPy]Br.....	68
Figure 4.2	<sup>1</sup> H NMR spectrum of [PPy]Br .....	70
Figure 4.3	<sup>13</sup> C NMR spectrum of [PPy]Br .....	70
Figure 4.4	(A) XRD patterns of samples after (a) 0 h (amorphous), (b) 16 h (amorphous + SAPO-34), (c) 19 h (SAPO-34) and (d) 30 h (SAPO-34 + SAPO-36) of hydrothermal treatment. The red asterisks in (d) show the presence of SAPO-34 as a minor competing phase for SAPO-36 (indicated by the black circles). (B) XRD pattern of A(c) after indexing and comparing with the theoretical CHA simulated pattern.....	73
Figure 4.5	FESEM micrographs of samples after (a, b) 0 h (amorphous), (c, d) 16 h (amorphous + SAPO-34), (e, f) 19 h (SAPO-34) and (g, h) 30 h (SAPO-34 + SAPO-36) of heating .....	74
Figure 4.6	IR spectra of samples after (a) 0 h (amorphous), (b) 16 h (amorphous + SAPO-34), (c) 19 h (SAPO-34) and (d) 30 h (SAPO-34 + SAPO-36) of hydrothermal treatment.....	76
Figure 4.7	Schematic illustration of the time-dependent formation of SAPO-34 in the presence of 1-propylpyridinium organic structural directing agent (OSDA) .....	76
Figure 4.8	(A) TG and (B) DTG plots of as-synthesized samples heated for (a) 0 h (amorphous), (b) 16 h (amorphous + SAPO-34), (c) 19 h (SAPO-34) and (d) 30 h (SAPO-34 + SAPO-36) .....	78
Figure 4.9	TG and DTG of pure [PPy]Br template .....	79
Figure 4.10	(a) Liquid state <sup>13</sup> C NMR spectrum of [PPy]Br, and (b) <sup>13</sup> C MAS NMR spectrum of as-synthesized SAPO-34 after crystallized for 19 h.....	80
Figure 4.11	Nitrogen adsorption-desorption isotherms of samples after (a) 0 h (amorphous), (b) 16 h (amorphous + SAPO-34), (c) 19 h (SAPO-34) and (d) 30 h (SAPO-34 + SAPO-36) of heating ..	81

Figure 4.12	NH <sub>3</sub> -TPD profiles (with deconvolution) of samples heated at (a) 0 h (amorphous), (b) 16 h (amorphous + SAPO-34), (c) 19 h (SAPO-34) and (d) 30 h (SAPO-34 + SAPO-36) .....	84
Figure 4.13	(A) XRD patterns of samples after (a) 16 h (amorphous), (b) 18 h (SAPO-34), (c) 20 h (SAPO-34 + SAPO-35) and (d) 21 h (SAPO-35). The asterisk in (c) corresponds to the diffraction peaks of SAPO-34. (B) XRD pattern of (d) after indexing and comparing with the theoretical LEV simulated pattern .....	87
Figure 4.14	FESEM images of samples after (a,b) 16 h (amorphous), (c,d) 18 h (SAPO-34), (e,f) 20 h (SAPO-34 + SAPO-35) and (g,h) 21 h (SAPO-35) .....	88
Figure 4.15	IR spectra of samples after (a) 16 h (Amorphous), (b) 18 h (SAPO-34), (c) 20 h (SAPO-34 + SAPO-35) and (d) 21 h (SAPO-35) .....	90
Figure 4.16	Schematic illustration of the time-dependent formation of SAPO-35 in the presence of 1-propylpyridinium organic structural directing agent.....	90
Figure 4.17	TGA/DTG of (a) pure [PPy]Br template and (b) as-synthesized SAPO-35.....	92
Figure 4.18	Nitrogen adsorption-desorption isotherm and porous properties of SAPO-35 .....	93
Figure 4.19	NH <sub>3</sub> -TPD profile of SAPO-35 crystallized using [PPy]OH at 200 °C for 21 h.....	94
Figure 4.20	The effect of the loading of SAPO-34 catalyst on the conversion of LA. Reaction conditions: temperature = 160 °C, time = 30 min, LA = 1.33 mmol, EtOH = 4.01 mmol, number of experiments = 2 .....	97
Figure 4.21	The effect of LA: EtOH molar ratios on the conversion of LA. Reaction conditions: temperature = 160 °C, time = 30 min, mass of SAPO-34 catalyst = 0.100 g, number of experiments = 2.....	98
Figure 4.22	Effect of reaction temperature and time on esterification of LA in the presence of (A) SAPO-34 and (B) SAPO-35. Reaction conditions: LA = 1.33 mmol, EtOH = 14.7 mmol, mass of catalyst = 0.100 g. Number of experiment = 2 .....	100
Figure 4.23	The Arrhenius plot of (a) SAPO-35 and (b) SAPO-34 catalysts for the esterification reaction between the levulinic acid and ethanol. Reaction conditions: LA = 1.33 mmol, EtOH = 14.7 mmol, mass of catalyst = 0.100 g .....	101

Figure 4.24	The effect of alcohol chain length and branching on the conversion of LA. Reaction conditions: Temperature = 190 °C, time = 20 min, LA = 1.33 mmol, alcohols = 14.7 mmol, mass of SAPO-34 catalyst = 0.100 g. Number of experiments = 2.....	102
Figure 4.25	Conversion of LA using various acid catalysts. Reaction conditions: Temperature = 190 °C, time = 20 min, LA = 1.33 mmol, EtOH = 14.7 mmol, mass of catalysts = 0.100 g (or equivalent to 46 μmol). Number of experiments = 2. SAPO <sup>a</sup> = TEAOH-SAPO-34 .....	104
Figure 4.26	Proposed mechanism for the esterification of LA into EL .....	106
Figure 4.27	Reusability study of (A) SAPO-34 and (B) SAPO-35 in 5 consecutive runs. Reaction temperature = 190 °C, time = 20 min, LA = 1.33 mmol, EtOH = 14.7 mmol, mass of catalysts = 0.100 g. Number of experiments = 2 .....	108

## LIST OF SYMBOLS, ABBREVIATIONS AND NOMENCLATURES

Å	Angstrom ( $1 \times 10^{-10}$ m)
AFI	AIPO Five
AIPO-n	Aluminophosphate-n
AIPO-5	Aluminophosphate-5
AST	AIPO Sixteen
ATT	AIPO Twelve-TAMU
ca.	Circa (approximately)
CHA	Chabazite
D4R	Double 4 ring
D6R	Double 6 ring
EMT	Ecole Mulhouse Chemistry number-2
FCC	Fluid catalytic cracking
H-LTL	H-Linde Type L
H-Y	H-Linde Type Y
HDO	Hydrodeoxygenation
IUPAC	International of Pure and Applied Chemistry
IZA	International Zeolite Association
Me <sup>+</sup>	Metal cations
MAS NMR	Magic angle spinning nuclear magnetic resonance
MOF	Metal organic framework
MOR	Morpholine
MR	Membered-ring
MTO	Methanol-to-olefins

PBUs	Primary building units
PIP	Piperidine
P/Po	Partial pressure
R	Ring
Rpm	Revolution per minute
S6R	Single six ring
SBUs	Secondary building units
SDAs	Structural-directing agents
SM	Substitution mechanism
Zr	Zirconium

**SINTESIS, PENCIRIAN DAN KAJIAN PEMANGKINAN MIKROLIANG  
SILIKOALUMINOFOSFAT DALAM PENGESTERAN ASID LEVULINIK  
DENGAN ETANOL**

**ABSTRAK**

Silikoaluminofosfat (SAPO-n) nombor 34 (SAPO-34) dan nombor 35 (SAPO-35) adalah zeolit berliang kecil dengan gelang lapan atom yang biasanya digunakan sebagai pemangkin dalam industri petrokimia. Namun begitu, kajian pembentukan berdasarkan masa penghabluran kedua-dua jenis zeolit tersebut jarang dikaji dan sintesis kedua-dua bahan ini memerlukan masa penghabluran yang panjang (sekurang-kurangnya 24 jam) kerana penggunaan agen pengarah struktur (SDA) organik amina. Projek ini memfokuskan kepada sintesis hidrotermal dan evolusi berdasarkan masa penghabluran SAPO-34 dan SAPO-35 dengan menggunakan SDA baharu 1-propilpiridinum hidroksida ([PPy]OH). Kajian mikroskopi dan spektroskopi menunjukkan bahawa induksi dan penukleasan berlaku sebelum pembentukan hablur SAPO-34 (200 °C, 19 jam) yang berubah sebahagian fasanya kepada SAPO-36 pada 30 jam, manakala SAPO-35 tulen (200 °C, 21 jam) diperoleh secara transformasi intrazeolit daripada SAPO-34. Khususnya, SAPO-34 dan SAPO-35 yang menggunakan [PPy]OH menunjukkan keliangan, kandungan silikon dan keasidan yang lebih tinggi berbanding dengan sistem templat yang lain. Hablur SAPO-34 dan SAPO-35 telah digunakan untuk memangkinkan pengesteran asid levulinik (LA) dengan etanol (EtOH) melalui kaedah pemanasan segera bukan gelombang mikro. SAPO-34 dan SAPO-35 masing-masing menunjukkan 93.4% dan 96.3% penukaran LA dengan 100% kepilihan terhadap etil levulinat pada 190 °C, 20 min. Kedua-dua mangkin tersebut menunjukkan kebolegunaan semula yang tinggi, iaitu sekurang-

kurangnya lima kitaran dan merupakan alternatif berpotensi dalam menggantikan mangkin asid homogen tradisional dalam tindak balas pengesteran.



**SYNTHESIS, CHARACTERIZATION AND CATALYTIC STUDY OF  
MICROPOROUS SILICOALUMINOPHOSPHATES IN THE  
ESTERIFICATION OF LEVULINIC ACID WITH ETHANOL**

**ABSTRACT**

Silicoaluminophosphate (SAPO-n) number 34 (SAPO-34) and number 35 (SAPO-35) are eight-membered small pore zeolites commonly used as catalysts in the petrochemical industry. However, the time-dependent formation study of these zeolites is rarely studied and their syntheses generally require long crystallization time (at least 24 h) due to the use of organic aminic structural directing agents (SDAs). This project focuses on the hydrothermal synthesis and time-dependent evolution of SAPO-34 and SAPO-35 using a novel 1-propylpyridinium hydroxide ([PPy]OH) SDA. The microscopic and spectroscopic investigations reveal that induction and nucleation precede the formation of fully crystalline SAPO-34 at 200 °C for 19 h which partially transformed into SAPO-36 at 30 h, while pure SAPO-35 (200 °C, 21 h) was obtained from the intrazeolite transformation from SAPO-34. Notably, the [PPy]OH-templated SAPO-34 and SAPO-35 show higher porosity, silicon content and acidity compared to other templating systems. The crystallized SAPO-34 and SAPO-35 were also used to catalyze the esterification of levulinic acid and ethanol under non-microwave instant heating method. The SAPO-34 and SAPO-35 show 93.4% and 96.3% LA conversion, respectively, with 100% selectivity to ethyl levulinate at 190 °C and 20 min. The catalysts also show excellent reusability for at least five cycles and are potential alternatives to the traditional homogenous acid catalysts in the esterification reaction.

# CHAPTER 1

## INTRODUCTION

### 1.1. General introduction

The looming possibility of an energy crisis in the future raises global awareness on the heavy reliance on fossil fuels. Since fossil fuels are limited in nature, these resources will become increasingly depleted and expensive. It is further aggravated by the increased demands from the industrialization of emerging economies, increasing world population and the high availability of various transportation means. Besides, the combustion of fossil fuel is notorious for its significant contribution to the environmental pollution and climate change especially by the emission of greenhouse gases, apart from the frequent fluctuation of the price of fossil fuel. Thus, global warming effect arises due to the failure of the emission of the thermal infrared rays into the space that consequently lead to the increase in the temperature of the Earth [1]. It is forecasted that the rate of worldwide emission of energy-related carbon dioxide (CO<sub>2</sub>) gases will increase at a rate of 1.6 percent annually reaching 140 billion metric tonnes in the year 2030 compared to the 114 billion metric tonnes in 2010 [2]. Furthermore, the global mean temperature has increased about 0.3-0.6 °C and a further maximum rise of 3.5 °C is expected by the year of 2100 with the concomitant rise in the global sea level based on the current rate of greenhouse gases released into the atmosphere [3]. Thus, biofuels could be an alternative to the conventional fossil fuels considering their renewable sources and environmental friendliness in reducing the emission of greenhouse gases [4].

Levulinate esters are one of the important biofuels besides being used as additives, solvents, plasticizers and fragrances [5]. In general, levulinate esters are synthesized through the esterification of levulinic acid with alcohols, where levulinic acid is a cheap and renewable reactant recognized as one of the twelve valuable biomass-derived platform chemicals [6]. Ethyl levulinate is especially industrially useful as biofuel additive. It is miscible with diesel up to 20 v/v(%) which reduces the dependence on the non-renewable fuel. Besides, it reinforces the stability and cold flow properties of the biodiesel, such as cloud point and pour point. Furthermore, the kinematic viscosities and flash point of the biofuels are improved upon the addition of ethyl levulinate which strengthen the engine effectiveness [7-9].

Traditionally, the esterification of levulinic acid is conducted under reflux conditions. As the reaction mixture is unable to be heated to temperature higher than their boiling points due to the open system, the reaction hence proceeds at a slow rate (hours or days). Besides, the heat transfer in the conventional reflux heating method is slow and inefficient as it depends on the thermal conductivity of materials used. Thus, the use of other heating methods, such as microwave heating, and non-microwave instant heating, that promotes homogeneous and rapid heat transfer with simple instrumental set-up is highly desirable. Furthermore, the esterification process is conventionally conducted in the presence of homogenous acid catalysts (HCl, H<sub>2</sub>SO<sub>4</sub>, H<sub>3</sub>PO<sub>4</sub>) at atmospheric pressure. However, homogeneous catalysis suffer from a couple of intrinsic problems associated with their high corrosiveness, poor catalysts separation and recovery, complicated post-treatment process and high waste disposal [10]. Hence, the replacement of these homogeneous catalysis with other eco-friendly and reusable catalysis are of utmost importance. Zeolitic materials are one of the heterogenous catalysis that have milder acidities compared to the conventional

homogenous acid catalysts. Hence, comparable reactivity as homogeneous catalysts with higher selectivity to the desired products in the catalytic reactions can be achieved while the drawbacks associated with homogeneous catalysts are eliminated.

Zeolites are hydrated crystalline three-dimensional microporous aluminosilicates linked together by the tetrahedral  $[\text{SiO}_4]$  and  $[\text{AlO}_4]^-$  through the sharing of the apical oxygen atom. The negative charge of the zeolite framework is balanced by cations that gives zeolites ion-exchanging ability and Brønsted acidity for catalytic reaction. On the other hand, aluminophosphate (AIPO-n) zeotype material consists of strictly alternating  $[\text{AlO}_4]^-$  and  $[\text{PO}_4]^+$  monomer units that makes the AIPO-n framework electrically neutral and catalytically inactive. The incorporation of silicon (Si) into the theoretical aluminophosphate (AIPO-n) framework results in a negatively-charged SAPO-n framework. Similar to zeolites, the net negative charge of SAPO-n framework is balanced by cations that makes it catalytically active. SAPO-n materials were first successfully synthesized by Lok et al. (1984) in the presence of organic structural directing agents (SDAs) [11]. SAPO-n materials have found broad industrial applications as adsorbents and in various industrial catalytic applications, such as methanol-to-olefins (MTO) reaction, hydroisomerization of long-chain paraffin [12, 13], dewaxing [14], isomerization [15], hydrodeoxygenation (HDO) of vegetable oils [16], *n*-alkane cracking [17] and oxidative dehydrogenation of ethane [18]. SAPO-34 is a three-dimensional eight-membered small pore zeotype that is currently the most promising catalyst in methanol-to-olefins reaction (MTO). Its synthesis usually requires the usage of organic aminic SDAs, such as tetraethylammonium hydroxide (TEAOH) [19], diethylamine (DEA) [20], morpholine (MOR) [21] and piperidine [22] for enabling crystallization at certain temperatures (180-200 °C) and long crystallization time (24 h-8 d). Akin to SAPO-34, SAPO-35 is a two-dimensional eight

membered zeotype that is mostly synthesized in the presence of hexamethyleneimine organic template. However, its hydrothermal synthesis requires a remarkable longer time to complete (24 h to 15 d) even at 200 °C.

Owing to the electronic delocalization at the pyridine heterocycle, the surface charge and electron density of the pyridinium molecule are always varying [23]. These pyridinium-based templates are expected to show different structural-directing behaviour compared to aliphatic template as they have unique structure, polarity, electron charge and hydrophobicity different from the traditional aliphatic aminic organic SDAs that further influence the zeotype crystallization process [24]. However, it is rare that pyridinium-based organic SDAs are synthesized and applied in the hydrothermal synthesis of zeotype materials. Consequently, the synthesis and time-dependent formation of SAPO-34 and SAPO-35 zeotypes in the presence of the pyridinium-based organic SDA are rarely investigated.

## **1.2. Research objectives**

This study aims to

- (a) Synthesize and characterize novel pyridinium-based organic SDA for the synthesis of SAPO-34 and SAPO-35 zeotypes.
- (b) Investigate of the time-dependent formations of SAPO-34 and SAPO-35 zeotypes in the presence of the novel pyridinium-based organic SDA.
- (c) Investigate the catalytic behaviour of the catalysts and optimize the reaction parameters in the esterification reaction of levulinic acid with ethanol using the non-microwave instant heating method.

### 1.3. Thesis outline

This thesis is composed of five chapters which provides an insight into the project background, literature survey, experimental procedures and a discussion on the research findings. Chapter 1 includes a brief overview into this project in which the research objectives, the background knowledge on the relevant zeotype materials and catalytic esterification process are introduced. A detailed and comprehensive literature review revolving around the fundamental concepts on zeolitic materials (SAPO-34 and SAPO-35), formation mechanisms and the roles of structural directing agents are elucidated in Chapter 2. Furthermore, a study into the weaknesses of the traditional catalytic esterification of levulinic acid, the potential applications of zeolites as solid acid catalysts and the non-microwave instant heating method are also presented.

Chapter 3 gives an account on the preparation of novel pyridinium-based organic template solution and its application in the synthesis and formation studies of SAPO- $n$  ( $n = 34$  and  $35$ ) zeotype materials. Besides, the basic principle of various characterization techniques employed in this project, such as X-ray diffraction analysis (XRD), thermogravimetry and differential thermal analysis (TG/DTA), Fourier transform infrared spectroscopy (FT-IR), field emission scanning electron microscopy (FESEM) and temperature programmed desorption of ammonia ( $\text{NH}_3$ -TPD) are also described herein. Lastly, the experimental procedure on the catalytic esterification of levulinic acid in the presence of solid acid catalysts using non-microwave instant heating method is also included.

A detailed presentation of experimental results and discussion form the core of Chapter 4 of this dissertation. This includes the synthesis and characterization of pyridinium-based organic template solution and the time-dependent formation study

of SAPO-34 and SAPO-35 materials in the presence of self-prepared organic template. Subsequently, solvent-free esterification of levulinic acid with ethanol under non-microwave instant heating method in the presence of SAPO-34 and SAPO-35 zeotype acid catalysts is also reported. Besides, the effects of various parameters on esterification process, such as molar ratio of levulinic acid to ethanol, heating modes (autoclave, conventional reflux heating, non-microwave instant heating method), reaction temperature and time are also studied and optimized.

Chapter 5 gives the conclusions derived from the experimental results and recommendations for future works are also given to broaden and deepen the development of microporous SAPO-n as solid acid catalyst in catalytic reactions.

## CHAPTER 2

### LITERATURE REVIEW

#### 2.1. Zeolites as microporous materials

Porous materials are generally defined as solids with continuous network that contain voids, *viz.* the volumes that are not occupied by the main framework atoms. The pores can be classified into open pores that connect to the external surfaces of materials and closed pores that are inside the materials which are inaccessible [25]. Open pores are preferable in industrial applications such as separation, bioreactors, adsorption and catalysis, while closed pores find more applications in thermal insulation and structural components with low density [26].

The International of Pure and Applied Chemistry (IUPAC) categorises porous materials based on their dimensions, namely micropores (<2 nm), mesopores (2-50 nm) and macropores (>50 nm) [27]. Microporous materials that have pore diameter less than 2 nm are important in many industrial applications (e.g. adsorption, molecular sieves and catalysis) due to their high porosity and surface area [28]. In addition, the presence of regular well-defined pores with specific shape creates shape- and size-based selectivities to the solids [29, 30]. These superior characteristics are shown by zeolite materials.



## **2.2. Zeolites and silicoaluminophosphate (SAPO-n) zeotype materials**

### **2.2.1. Zeolites**

The term “zeolite” originates from Greek in which “zeo” means “to boil” and “lithos” means “stones”. Zeolite was first discovered by a Swedish mineralogist, Alex Fredrik Cronstedt, by which the mineral was later named stilbite [31]. However, it was Richard Barrer who successfully synthesized the first zeolite without natural counterpart [32]. Since then, the first large-scale methodology for hydrothermal zeolite synthesis was pioneered by Robert Milton and co-workers at the Union Carbide laboratories in 1949 at low temperature (*ca.* 100 °C) and autogenous pressure in the presence of alkali metal cations leading to the discovery of zeolites A and X [33]. Earlier works have focused on the use of inorganic cations ( $\text{Na}^+$ ,  $\text{K}^+$ ) as structural directing agents such as in the synthesis of ZK-4 zeolite [34].

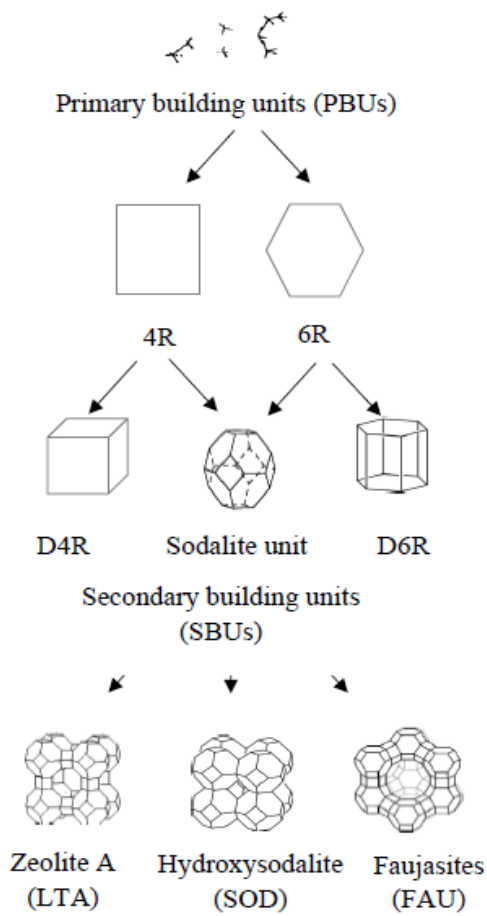
The next major advance in the synthesis of zeolites was brought about by the application of organic components, such as alkylamines and alkylammonium salts, as space filling species, structural directing agents and templates [35]. The introduction of organic templates enables the synthesis of high silica zeolites (high Si/Al ratio) as only a limited number of bulky organic molecules can be occluded into the zeolite pores compared to the inorganic cations. Thereafter, it led to the discovery of the first high silica beta zeolite using tetraethylammonium hydroxide [36] and the pure siliceous ZSM-5 zeolite using tetrapropylammonium hydroxide [37]. A mixture of organic amines and metal ions was also applied to synthesize ZK-4 zeolite [38].

In general, zeolites are hydrated aluminosilicate crystalline materials that consist of three-dimensional microporous channels. The primary building units (PBUs) of zeolites are tetrahedrally-linked  $[\text{SiO}_4]$  and  $[\text{AlO}_4]^-$  where the random combinations of these PBUs then form the secondary building units (SBU) [39]. The multiple ways

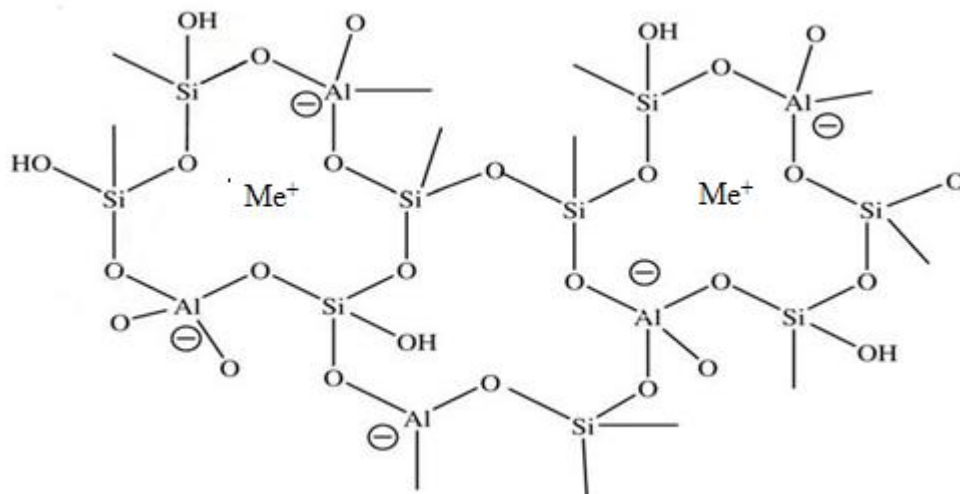
of joining these SBUs eventually lead to a variety of different zeolite frameworks that are denoted by a three-letter code assigned by the International Zeolite Association (IZA) (Figure 2.1) [40-42].

The general formula of zeolites is  $M_{X/N}(AlO_2)_X(SiO_2)_Y \cdot nH_2O$ , where N represents the valency of the cations, X and Y are the numbers of tetrahedral unit cells, M is the non-framework cations and n is the number of moles of the chemisorbed water [43]. Due to the incorporation of trivalent aluminum atoms, an overall negative charge is induced on the zeolite framework that needs to be counter balanced by the extraframework metal cations ( $Me^+$ ) (Figure 2.2) [44].

The presence of extraframework cations enables the formation of Brønsted acid sites which impart zeolites important commercial and industrial values [43]. Besides, zeolites are highly porous materials that have pores of molecular dimension ( $< 20 \text{ \AA}$ ) with various shapes and sizes giving rise to their shape selectivity [29]. These properties thus explain the significance of zeolites in various industrial applications, particularly in the petrochemical industry (Table 2.1) [30, 43, 45].



**Figure 2.1.** The random combination of primary building units (PBUs) into the secondary building units (SBUs) and the connection among the SBUs into zeolites of different framework types (R = ring, D4R = double 4 ring, D6R = double 6 ring) [46].



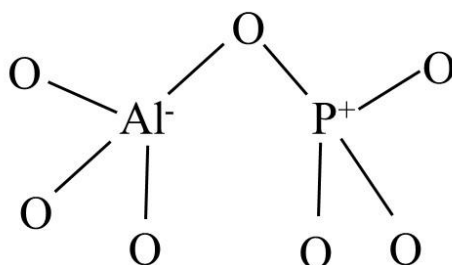
**Figure 2.2.** A general two-dimensional structure of a zeolite framework [47].

**Table 2.1.** The industrial applications of zeolites [45].

<b>Zeolite structures</b>	<b>Zeolites</b>	<b>Pore apertures (Å)</b>	<b>Applications</b>
FAU	Y	7.4	Cracking (FCC) Hydrocracking of oil Alkylation of aromatics
BEA	Beta	$7.6 \times 6.4$	Synthesis of ethyl benzene and cumene
LTL	K-L	7.1	Aromatization
MOR	Mordenite	$7.0 \times 6.5$	Hydroisomerization of <i>n</i> -Paraffin, transalkylation of aromatics, cumene synthesis
MFI	ZSM-5	$5.3 \times 5.6$	FCC, dewaxing, aromatization, xylene hydroisomerization, toluene disproportionation, ethylene-benzene alkylation
	Silicalite	$5.1 \times 5.5$	Methanol to fuels or light olefins
AEL	SAPO-11	$3.9 \times 6.3$	Isodewaxing
TON	ZSM-22	$4.4 \times 5.5$	Isodewaxing
MWW	MCM-22	$5.5 \times 4.0$	Synthesis of ethyl benzene and cumene
FER	Ferrierite	$4.2 \times 5.4$ $3.5 \times 4.8$	Butene hydroisomerization
CHA	SAPO-34	$3.8 \times 3.8$	Methanol-to-olefin (MTO) conversion

### 2.2.2. Aluminophosphate (AIPO-n) and silicoaluminophosphate (SAPO-n) zeotypes

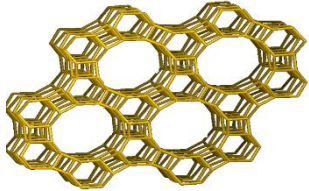
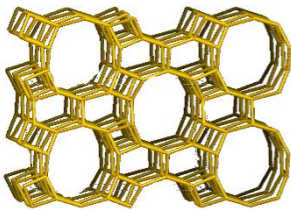
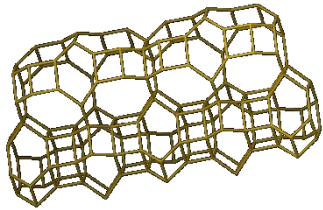
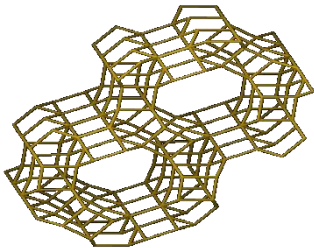
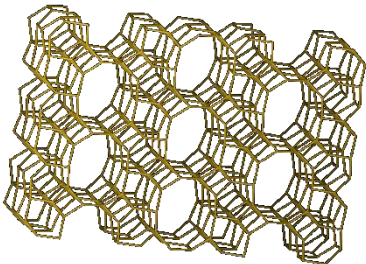
Aluminophosphates (AIPO-n) are zeolite-like materials. Wilson et al. (1982) reported the first successful hydrothermal synthesis of AIPO-n without silicon. The AIPO-n zeotypes are not naturally found and their synthesis requires the presence of structural directing agents which are usually organic amines and quaternary ammonium ions [48]. Unlike zeolites, AIPO-n are electrically neutral due to the arrangement of strictly alternating  $[\text{AlO}_4]^-$  and  $[\text{PO}_4]^+$  monomer units that must be in obedience to the Lowenstein's rule (Figure 2.3) [48-50]. Besides, Flanigen et al. (1988) also eliminates the possibility of P-O-P linkages due to their energy instability and the formation of an overall positive zeotype framework [51]. Hence, the framework composition of aluminophosphate zeotypes is always  $\text{Al/P} = 1$  under these restrictions.



**Figure 2.3.** A neutral framework of aluminophosphate (AIPO-n) with alternating  $[\text{AlO}_4]^-$  and  $[\text{PO}_4]^+$  monomer units [51].

So far, more than 50 types of AIPO-n with novel unique structures have successfully been synthesized with extra-large pores (>12 rings), large pores (12 rings), medium pores (10 rings), small pores (8 rings) and very small pores (6 rings) (Table 2.2) [52].

**Table 2.2.** The structure types, pore sizes and pore openings of several AlPO-*n* [42].

AlPO- <i>n</i>	Structure type	Pore size (Å <sup>2</sup> )	Pore opening	Framework structure
<i>n</i> = 5	AFI	7.3 × 7.3	12	
<i>n</i> = 11	AEL	4.0 × 6.5	10	
<i>n</i> = 17	ERI	3.6 × 5.1	8	
<i>n</i> = 31	ATO	5.4 × 5.4	12	
<i>n</i> = 41	AFO	4.3 × 7.0	10	

Recently, the incorporation of elements other than aluminum and silicon, such as manganese [53], gallium [54], germanium [55], magnesium and cobalt [56] into the zeolite frameworks has gathered widespread attention due to their comparable pore volumes, uniform pore sizes and high surface areas with emerging new properties. The introduction of silicon into the aluminophosphate framework produces silicoaluminophosphates (SAPO-n) zeotype materials. SAPO-n materials were first synthesized hydrothermally in the presence of organic amines or quaternary ammoniums as structural directing agents [11]. These materials exhibit excellent (hydro)thermal stability, uniform pore size with milder acidity compared to their zeolites counterpart enabling their application in size- and shape-selective separation and catalysis reactions [11, 57]. So far, the SAPO-n materials have been used as adsorbents and catalysts in various industrial applications, such as methanol to olefins (MTO) reaction, the hydroisomerization of long-chain paraffin [12, 13], dewaxing [14], isomerization [15], hydrodeoxygenation (HDO) of vegetable oils [16], *n*-alkane cracking [17] and oxidative dehydrogenation of ethane [18].

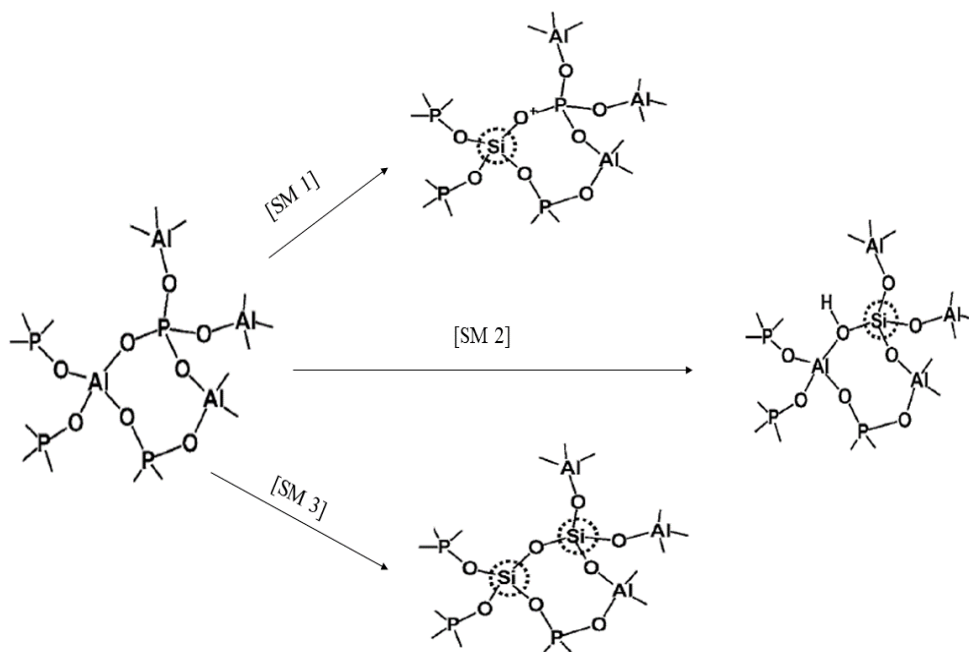
### **2.2.3. Mechanism of Si insertion**

The isomorphic substitution of silicon for either phosphorus or aluminum or both produces the SAPO-n zeotypes framework. It is achieved through the addition of silicon elements into the AIPO-n mixture. There are three proposed substitution mechanisms (SM) for the incorporation of silicon into the AIPO-n framework, namely the substitution of silicon for aluminum (SM1), the substitution of silicon for phosphorus (SM2) and the substitution of two silicons for a pair of aluminum and phosphorus (SM3) [58]. However, the substitution of silicon for aluminum (SM1)

generates P-O-Si linkages and an overall neutral SAPO-n framework which is thermodynamically undesirable [51].

In general, the substitution of silicon follows a mixture of SM2 and SM3. The substitution of silicon for phosphorus (SM2) in the neutral AIPO framework generates a net overall negative charge on the SAPO-n zeotype framework that leads to the production of Brønsted acid sites and ion-exchanging capability of SAPO-n materials. Apart from that, substituting a pair of phosphorus and aluminum by silicons generates unstable Si-O-P bonds *via* SM 3 mechanism. Hence, SM 3 mechanism is often accompanied by SM 2 mechanism where the immediate neighbours of silicons are either themselves or aluminum. It generates siliceous islands that only Si-O-Si and Si-O-Al linkages are observed [58-62]. In addition, the use of organic structural directing agents (SDAs) during the synthesis of SAPO-n zeotype materials affects the mechanism of silicon incorporation. As organic SDAs also play a charge-compensating role, the charge introduced by silicon substitution cannot exceed those provided by the occluded templates in the zeotype framework [58-62]. Figure 2.4 illustrates the three substitution mechanisms of silicon into the AIPO-n zeotype framework.



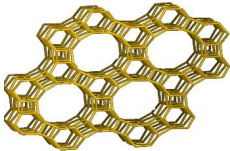
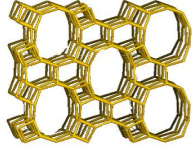
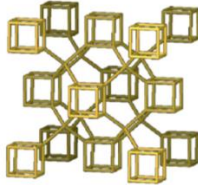
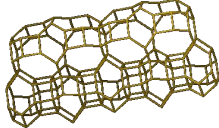
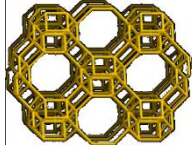
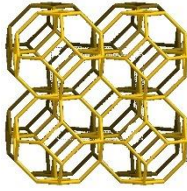
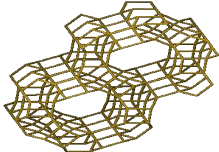



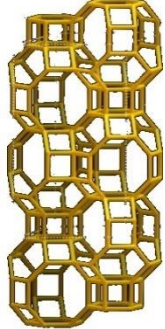
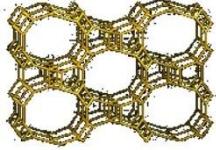
**Figure 2.4.** Three substitution mechanisms of silicon into a AlPO-*n* framework [61].

#### 2.2.4. Structural building units, topology codes and framework structures

Aluminophosphate and silicoaluminophosphate materials are named by the International Zeolite Association based on the unique framework types. There exists a corresponding silicoaluminophosphate analogue for every aluminophosphate framework since both materials possess identical topology. Each zeotype is designated AlPO-*n* and SAPO-*n* where *n* is an integer that denotes their unique framework type followed by a three-letter code. For example, framework code AFI (AlPO Five) is assigned to AlPO-5 and SAPO-5 while ATS (AlPO Thirty-Six) is assigned to AlPO-36 and SAPO-36. However, certain zeotypes are named after their zeolite analogues. For example, AlPO-34 and SAPO-34 are named after zeolite CHA [42]. Table 2.3. shows some SAPO-*n* materials with their respective structure codes, ring openings, pore sizes and framework structures.

**Table 2.3.** Some SAPO-n materials with their respective structure codes, ring openings and framework structure [63].

SAPO-n	Structure code	Number of membered ring	Pore size ( $\text{\AA}^2$ )	Framework structure
SAPO-5	AFI	12	$7.3 \times 7.3$	
SAPO-11	AEL	10	$4.0 \times 6.5$	
SAPO-16	AST	6	-	
SAPO-17	ERI	8	$3.6 \times 5.1$	
SAPO-18	AEI	8	$3.8 \times 3.8$	
SAPO-20	SOD	6	$2.8 \times 2.8$	
SAPO-31	ATO	12	$5.4 \times 5.4$	
SAPO-34	CHA	8	$3.8 \times 3.8$	

SAPO-35	LEV	8	$3.6 \times 4.8$	
SAPO-36	ATS	12	$6.5 \times 7.5$	

### 2.2.5. Comparison between zeolites and SAPO-n zeotype materials

Aluminosilicate zeolites are usually synthesized in an alkaline medium (pH 9-14) [64]. The synthesis gels with lower pH may lead to the formation of dense phase aluminosilicates. However, the synthesis of SAPO-n shows preference towards a weakly acidic or neutral medium (pH 6-8) [61].

The aluminum sources for zeolites and SAPO-n materials are usually acquired from aluminum hydroxides, aluminum alkoxides and pseudoboehmite. While both zeolites and SAPO-n use the same silica sources (e.g. fumed silica, colloidal silica, tetraorthosilicate (TEOS)) for the syntheses, the phosphorus source in SAPO-n mostly originates from orthophosphoric acid. Hence, the pH of SAPO-n precursor gels is weakly acidic or neutral while that of zeolite tends to be more basic. Furthermore, the reaction pH is also affected by the usage of template or organic SDAs.

SAPO-n frameworks are negatively charged similar to zeolites due to the incorporation of tetravalent silicon into the AlPO-n framework that generate Brønsted acid sites. As a result, SAPO-n materials are catalytically active as compared to their AlPO-n counterparts. However, the acidity of SAPO-n is weaker than the zeolites [57]. The comparison between zeolites and SAPO-n are summarized in Table 2.4.

**Table 2.4.** A comparison between the zeolites and the SAPO-n zeotypes.

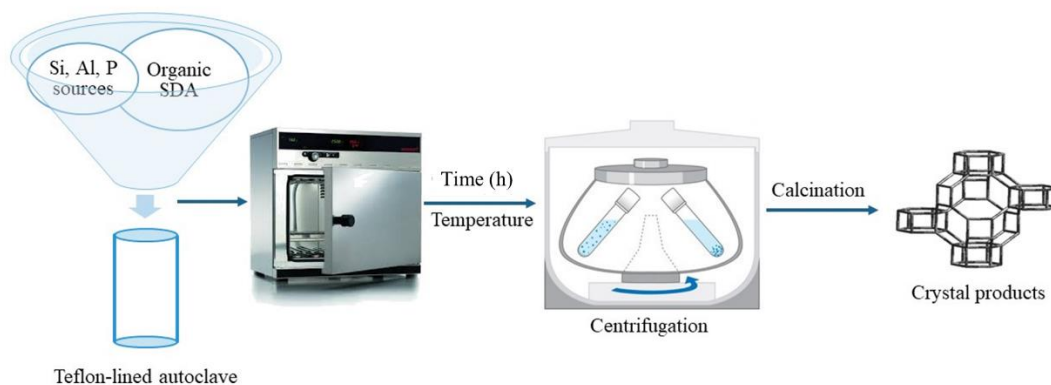
<b>Characteristics</b>	<b>Zeolites</b>	<b>SAPO-n</b>
Precursor composition	The precursor gels contain aluminosilicates	The precursor gels contain silicoaluminophosphates
Framework composition	The framework consists of aluminum and silicon atoms	The framework consists of aluminum, silicon and phosphorus atoms.
Precursor sources	Aluminum sources mostly are derived from aluminum hydroxide, aluminum alkoxides and pseudoboehmite while silica sources are from fumed silica, colloidal silica and TEOS.	Aluminum sources mostly are derived from aluminum hydroxide, aluminum alkoxides and pseudoboehmite while silica sources from fumed silica, colloidal silica and TEOS. However, orthophosphoric acid usually contributes the phosphorus source in SAPO-n synthesis.
Framework formation	The introduction of aluminum generates an overall net negative charge which is compensated by organic SDAs or inorganic cations.	The introduction of silicon generates an overall negative charge which is compensated by organic SDAs.
pH of the precursor gel	A highly basic medium is needed for synthesis.	A weakly acidic or neutral medium is needed for synthesis.

Strength of Brønsted sites	Stronger acid	Stronger	Milder
Types of linkages	Presence of Si-O-Si and Si-O-Al linkages only. The Al-O-Al linkages are forbidden (Lowenstein's rule).	The Al-O-Al bonds (Lowenstein's rule) and P-O-P bonds (Flanigen's rule) are avoided.	

### 2.3. Hydrothermal synthesis

The hydrothermal synthesis of SAPO-n is nearly similar to that of zeolites, but their crystallization occurs in a weakly acidic or neutral medium. Typically, the synthesis of SAPO-n zeotypes begins with the mixing of aluminum, phosphorus and silica sources in the presence of organic SDA under continuous stirring in water to obtain a homogenous aqueous mixture. The mixture is then transferred into a Teflon vessel and subjected to heating (100-250 °C) for a specific period (hours to days) under autogenous pressure [65].

During the induction period, the reactant mixture will remain amorphous for a certain period. Subsequently, nucleation and crystallization ensue until the initial amorphous solids are transformed into crystals of approximately equivalent mass. The crystals are then recovered from the mother liquor by filtration or centrifugation, washed thoroughly with distilled water and dried in an oven [65]. The crystalline solids are then subjected to calcination at high temperature (~550 °C) to remove the organic SDA encapsulated in the pores of SAPO-n. The common procedure in the hydrothermal synthesis of SAPO-n zeotypes is summarized in Figure 2.5.



**Figure 2.5.** Schematic diagram of the preparation procedure and the hydrothermal synthesis of SAPO-n zeotypes.

### 2.3.1. Effect of synthesis parameters

The SAPO-n formation is influenced by several parameters, such as the reactant composition, synthesis time, crystallization temperature, autogenous pressure generated, aging, pH and the type of organic SDA used. Changes in the  $P_2O_5$  to  $Al_2O_3$  ratio (P/Al ratio) and content affect the product yield, crystallinity, framework composition and type of framework structure formed. Auwal et al. (2021) discovered that a higher P/Al ratio increases the crystallinity in the zeotype formed [66]. Besides, a higher P/Al ratio also contributes to the formation of crystals of large size [67-69].

The molar ratios of water and hydroxide ions are also significant parameters due to their role as mineralizing agents [70]. Hence, it is expected that high concentrations of water and hydroxide ions improve the nucleation and crystallization rates due to an increase in the hydrolysis rate of the precursor mixtures. The concentration of water in the reaction mixture is also found to affect the morphology of the zeotype formed. It was discovered that as the reaction mixture becomes more diluted, the morphology of the AIPO-5 zeotype changes from spherical agglomerates with minute flake-like crystallites to columnar-like morphology [71]. A higher concentration of water also resulted in the decrease in the surface area and micropore

volume and an increase in mesoporosity and crystal size [69, 71, 72]. Another study into the effect of water content reveals that AST zeotype tends to be the predominant phase at low water concentrations while ATT zeotype forms as an impurity phase along with the AFI zeotype at high water concentration [73].

In addition, the pH of synthesis precursor is important in the SAPO-n synthesis. Under acidic conditions, crystalline SAPO-n phase is predominant while the formation of amorphous phase is expected under alkaline condition [72, 74]. As the phosphorus source in the synthesis of SAPO-n zeotype materials is often derived from orthophosphoric acid, the pH of the reactant mixture could be increased to nearly neutral or weakly acidic by dilution through the addition of water and the alkaline organic SDA. However, the different pH of the reactant mixture may crystalline SAPO-n of different phases. At higher pH (7-8), it favours the formation of SAPO-34 (CHA) while SAPO-5 (AFI) tends to predominate at lower pH (5-6) [75-77].

High temperature and autogenous pressure improve the solvating capability of water in the hydrothermal synthesis of SAPO-n. Both factors facilitate the dissolution and mixing of the reactants which expedite the crystallization rate [78]. In addition, the synthesis temperature is also a significant parameter in determining the type of structure in the zeotype synthesis as it affects the self-generated pressure of water in the system. Auwal et al. (2021) found that increasing the synthesis temperature from 100 °C to 150 °C witnesses a phase transformation from amorphous to fully crystalline SAPO-5. However, further heating to 200 °C yielded tridymite dense phase [66]. Besides, low synthesis temperature generally yields zeolites with lower intercrystalline void space such as zeolites A and X [79]. However, higher synthesis temperature (>200 °C) will produce dense phases due to the increment in the autogenous pressure

generated [79]. Also, raising the synthesis temperature increases the crystal sizes as crystal growth rate increases more than nucleation at higher temperature [80].

### **2.3.2. Roles of organic SDAs**

Organic aminic SDAs are frequently used in the synthesis of SAPO-n zeotypes due to their ability to direct the formation of certain types of molecular sieves. In SAPO-n systems, organic SDAs are invariably needed for synthesis, such as tetramethylammonium hydroxide (TMAOH) in the synthesis of SAPO-37 [81], tetraethylammonium hydroxide (TEAOH) and diethylamine (DEA) in the synthesis of SAPO-34 [82, 83], tetrapropylammonium hydroxide (TPAOH) in the synthesis of SAPO-5 [84] and di-*n*-propylamine in the synthesis of SAPO-11 [85]

In general, the organic guest molecules function in three different ways during the SAPO-n synthesis, namely as (i) space fillers, (ii) structural directing agents (SDAs) and (iii) true templates [86]. Space fillers stabilize the growing molecular sieves by occupying the pores and voids in the framework. This reduces unfavourable energetic interaction between water solvent and the framework [79]. Meanwhile, SDAs are more specific in directing the formation of a specific framework types which are inaccessible to the other types of organic SDAs. A high correlation between the size and shape of organic SDAs and the resultant framework types was discovered [87, 88]. This remarkable geometrical correlation is due to the maximized van der Waals interaction between the framework and the organic species that stabilizes the zeolite structure [87, 88]. It is also found that an organic template may display a certain preference to a specific type of void or framework structure implying the structural-determining role of the organic template used. An example of structural direction of organic species is



shown in the synthesis of hexagonal Faujasite (EMT) through the action of crown ether 18-crown-6 [89].

The difference between a space filler and a structural directing agent is marked by the specificity of the organic template in the synthesis of zeolite and zeotype materials. As an example, the synthesis of AlPO-5, which shows a very minimal template selectivity, is made possible with the use of more than 20 types of organic species, such as imidazolium [67, 90], tripropylamine (TPA) [68], triethylamine (TEA) [91], tetraethylammonium hydroxide (TEAOH) [92], tetrabutylammonium hydroxide (TBAOH) [93], tetrapropylammonium hydroxide (TPAOH) [94] and N-methyldicyclohexylamine [95]. These organic templates function more as a space filler rather than a SDA since the same AlPO-5 structure is formed. However, different morphologies of AlPO-5 crystals were obtained for different SDAs, such as hexagonal prism structure, flower-like, rod-like structure and barrel-like structure [93, 96-98]. Besides, it is also possible that a single organic template can direct the formation of different framework types. As an example, dipropylamine (DPA) enables the synthesis of more than 5 different zeotype structures, such as AlPO-11 and SAPO-11 (AEL), VPI-5 (VFI), SAPO-5 (AFI) and SAPO-31 [85, 99, 100]. In short, organic species are essential in the synthesis of AlPO-n and SAPO-n zeotypes due to several reasons below:

- (a) Promoting and enabling the formation of certain types of molecular sieves.
- (b) Increasing the thermodynamical stability by packing into the cages and channels of the framework.
- (c) Modifying the gel chemistry to facilitate the occurrence of templating effect.
- (d) Increasing the nucleation and crystallization rates.